УДК 578.76
DOI: https://doi.org/10.17816/MAJ109066

COMPARATIVE STUDY OF THE PATHOGENICITY OF SARS-CoV-2 B.1 AND B.1.617.2 LINEAGES FOR SYRIAN HAMSTERS

Kirill S. Yakovlev[1], Daria A. Mezhenskaya[2], Konstantin V. Sivak[1], Larisa G. Rudenko[2], Irina N. Isakova-Sivak[2]

[1] Smorodintsev Research Institute of Influenza, Saint Petersburg, Russia;
[2] Institute of Experimental Medicine, Saint Petersburg, Russia

For citation: Yakovlev KS, Mezhenskaya DA, Sivak KV, Rudenko LG, Isakova-Sivak IN. Comparative study of the pathogenicity of SARS-CoV-2 B.1 and B.1.617.2 lineages for Syrian hamsters. *Medical Academic Journal.* 2022;22(2):125–136. DOI: https://doi.org/10.17816/MAJ109066

Received: 26.05.2022 Accepted: 03.06.2022 Published: 30.06.2022

BACKGROUND: Syrian hamsters are the most sensitive model for studying the pathogenesis of a new coronavirus infection and testing prophylactic and therapeutic drugs against SARS-CoV-2. Accordingly, it is important to identify pathomorphological indicators of tissue damage in coronavirus-infected animals, which would correlate with the severity of the disease.

AIM: Comprehensive assessment of the pathogenicity of SARS-CoV-2 viruses of B.1 and B.1.167.2 lineages on the model of Syrian hamsters to identify the most sensitive criteria that correlate with the clinical manifestation of the disease.

MATERIALS AND METHODS: Intranasal infection of animals with SARS-CoV-2, followed by the assessment of the clinical picture of the disease and detailed pathomorphological studies of various organs collected on the 5th day after infection.

RESULTS: The SARS-CoV-2 Delta virus (B.1.617.2) was shown to be less pathogenic for Syrian hamsters compared to the ancestral strain that circulated during the first wave of the COVID-19 pandemic (B.1). The histopathological characterization of lung tissue sections of infected animals revealed the most sensitive morphometric indicator that correlates with the severity of SARS-CoV-2-induced pathology, namely, the alveolar wall thickness.

CONCLUSIONS: The use of the alveolar thickness indicator makes it possible to determine even slight differences in the severity of virus-induced pathology in the Syrian hamster model, which can be critical in the preclinical evaluation of prophylactic and therapeutic drugs for COVID-19.

Keywords: coronavirus; SARS-CoV-2; Syrian hamsters; pathomorphology; lung pathology; morphometry.

СРАВНИТЕЛЬНЫЙ АНАЛИЗ ПАТОГЕННОСТИ ВИРУСОВ SARS-CoV-2 ГЕНЕТИЧЕСКИХ ЛИНИЙ B.1 И B.1.617.2 НА МОДЕЛИ СИРИЙСКИХ ХОМЯКОВ

К.С. Яковлев[1], Д.А. Меженская[2], К.В. Сивак[1], Л.Г. Руденко[2], И.Н. Исакова-Сивак[2]

[1] Научно-исследовательский институт гриппа имени А.А. Смородинцева, Санкт-Петербург, Россия;
[2] Институт экспериментальной медицины, Санкт-Петербург, Россия

Для цитирования: Яковлев К.С., Меженская Д.А., Сивак К.В., Руденко Л.Г., Исакова-Сивак И.Н. Сравнительный анализ патогенности вирусов SARS-CoV-2 генетических линий B.1 и B.1.617.2 на модели сирийских хомяков // Медицинский академический журнал. 2022. Т. 22. № 2. С. 125–136. DOI: https://doi.org/10.17816/MAJ109066

Рукопись получена: 26.05.2022 Рукопись одобрена: 03.06.2022 Опубликована: 30.06.2022

Обоснование. Сирийские хомяки — наиболее адекватная модель для изучения патогенеза новой коронавирусной инфекции и тестирования профилактических и терапевтических препаратов от SARS-CoV-2, так как они отличаются высокой чувствительностью к заражению этим вирусом. Таким образом, анализ корреляции тяжести заболевания с патоморфологическими признаками поражения тканей животных открывает новые возможности для оценки лекарственных средств в доклинической практике.

Цель статьи — комплексная оценка патогенности вирусов SARS-CoV-2 линий B.1 и B.1.167.2 на модели сирийских хомяков для выявления наиболее чувствительных критериев, коррелирующих с клинической картиной заболевания.

Материалы и методы. Интраназальное заражение животных вирусами с последующей оценкой клинической картины заболевания и детальным патоморфологическим исследованием различных органов, извлеченных на 5-е сутки после заражения.

Результаты. Показано, что вирус SARS-CoV-2 варианта Дельта (B.1.617.2) отличается меньшей патогенностью по сравнению с исходным штаммом B.1 первой волны пандемии COVID-19. Комплексное морфометрическое и гистологическое исследование тканей легких зараженных животных выявило наиболее чувствительный морфометрический показатель, отражающий степень выраженности SARS-CoV-2-индуцированной патологии — толщину межальвеолярных перегородок.

Заключение. Изменение толщины межальвеолярных перегородок позволяет определить даже незначительные различия в степени выраженности вирусиндуцированной патологии у сирийских хомяков, что может оказаться критическим при доклиническом исследовании препаратов от COVID-19.

Ключевые слова: коронавирус; SARS-CoV-2; сирийские хомяки; патоморфология; патология легких; морфометрия.

List of abbreviations

PBS, phosphate-buffered saline; MLI, mean linear interval.

Background

Severe acute respiratory syndrome coronavirus 2 (SARS-CoV-2), first identified in humans at the end of 2019 [1], caused a coronavirus disease 2019 (COVID-19) pandemic that has claimed the lives of more than 6 million people so far [2]. Soon after the identification of the pathogen, large-scale studies of the pathogenesis of the infectious process were started, including work on the creation of effective and safe therapeutic and prophylactic drugs. In addition to key virological techniques *in vitro* and *ex vivo*, studies using animal models have enabled assessment of the physiological significance of established links in pathogenesis [3]. Thus, it became necessary to identify infection-sensitive laboratory animals that can most accurately reproduce the clinical and laboratory presentation of human coronavirus infection.

Numerous experiments have demonstrated that Syrian hamsters represent as the optimal experimental model of SARS-CoV-2 infection for the preclinical assessment of the activities of antiviral drugs and vaccine candidates. This is primarily due to the ability of the desired coronavirus strains to replicate in the epithelium of the respiratory tract of hamsters, inducing lung damage characteristic of COVID-19 [3–7].

According to literature data, the assessment of the pathogenicity of SARS-CoV-2 variants in the Syrian hamster model is limited to monitoring changes in animal body weight, determining the viral load in respiratory organs, and assessing pathomorphological changes in lung tissues at baseline, expressed as a total score [7–9].

SARS-CoV-2 strains belonging to different genetic lineages can differ significantly in their ability to cause clinical symptoms and pathological changes in the respiratory tract in Syrian hamsters [10, 11]. This aspect can be used as the basis for determining the most sensitive morphometric criterion for assessing viral pathology. In the future, these indicators may be used to assess the efficiency of vaccines and therapeutic drugs.

This study aimed to identify the most sensitive morphological criteria for a comprehensive assessment of the pathogenicity of SARS-CoV-2 lines B.1 and B.1.167.2 in Syrian hamsters.

Materials and methods

SARS-CoV-2 strains isolated from COVID-19 in St. Petersburg were obtained from the collection of the Smorodintsev Research Institute of Influenza (St. Petersburg, Russia). We used the original SARS-CoV-2 B.1 strain circulating during the first wave of the pandemic at the beginning of 2020 (Accession no. in the GISAID database: EPI_ISL_415710) and the B.1.617.2 strain (Delta, GISAID: EPI_ISL_1789542) that appeared in 2021. SARS-CoV-2 isolates were accumulated on Vero cells (ATCC CCL-81) cultured in Dulbecco's modified Eagles medium (DMEM) supplemented with 2% fetal bovine serum (FBS), 1× antimycotic antibiotic, and 10 mM HEPES (all components manufactured by Gibco, USA) [DMEM/FBS] at 37°C, in an atmosphere of 5% CO_2 [12]. Cells were infected with viruses at a multiplicity of infection of 0.005 or 0.01 for strains B.1 and B.1.617.2, respectively [13]. After 72 h of incubation, the supernatant was collected, centrifuged at 2000 g for 15 min, aliquoted, and stored at −70°C.

Infectious titers of SARS-CoV-2 were determined by titrating the virus-containing fluid on 96-well plates seeded with Vero-CCL81 cells, and the 50% tissue culture infectious dose ($TCID_{50}$) was calculated. Tenfold dilutions of the virus prepared in DMEM/FBS medium were added to the wells and incubated at 37°C and 5% CO_2 for 72 h. Virus-infected wells were determined visually by the presence of a cytopathic effect. Infectious titer was calculated according to the Reed–Muench method, expressed as $\log_{10}$ $TCID_{50}$/mL [14]. All procedures with live SARS-CoV-2 isolates were performed in a BSL-3 biosafety level laboratory.

Golden Syrian hamsters (*Mesocricetus auratus*) were purchased from the nursery of the Scientific Center for Biomedical Technologies of the Federal Medical and Biological Agency, Stolbovaya branch. The animals were kept under standard laboratory vivarium conditions, with free access to food and water. The study was conducted in accordance with the Directive 2010/63/EU [15].

Animals aged 10 weeks and weighing 140–160 g (three individuals per group) were infected intranasally with 100 μL of virus-containing suspension, dose 10^5 $TCID_{50}$, under brief ether anesthesia. The control group of animals received phosphate-buffered saline (PBS) solution. Within 5 days after infection, the clinical symptoms and body weight changes were monitored. The clinical manifestation of the disease course was assessed in points according to certain criteria, namely, appearance and coat condition (0, normal; 1, lack of care), interaction with other animals (0, normal; 1, reduced), food consumption (0, normal; 1, reduced), behavior in an open space (0, active; 1, reduced), and reaction picking up (0, normal; 1, reduced).

On day 5, to assess the level of virus replication, the animals were sacrificed by an overdose of ether,

and the trachea, lungs, brain, liver, and kidneys were aseptically collected. Nasal tissues were collected only for virological studies. Before organ harvesting, the lungs were perfused with 10 mL of PBS through the right ventricle. Primarily, pathological changes were assessed macroscopically. One lung lobe was used for histopathological analysis. The remaining tissue was weighed and homogenized to determine the viral load by titration on Vero cells.

Organ fragments taken for histological studies were fixed in 10% buffered formalin solution (pH = 7.4) for 48 h. After obtaining the necessary sections, routine histological processing was applied on a Histo-Tek VP1 histoprocessor (Sakura, Japan), and samples were then embedded in paraffin blocks. The prepared sections with a thickness of 3 μm were stained with a hematoxylin and eosin solution. Microscopic examination was performed on a LEICA DM1000 light microscope. Measurements and photofixation were performed using the ADF Image Capture 4.17 software package.

Morphometric assessment of lung tissues included planimetry of the inflammatory lesion at ×50 magnification (ocular ×10; lens ×5). The lesion area was expressed as a percentage of the total section area. The dimensions of the air space were estimated using the mean linear interval (MLI). The intervals were calculated between the points of intersection of 10 parallel test lines with the walls of the alveoli and alveolar ducts in 10 random non-intersecting fields of view at a magnification of ×200 (ocular ×10; lens ×20). Septa, stroma, vessels with diameter >20 μm, and areas of lung tissue compression were excluded from the analysis [16]. Then, without changing the field of view and magnification, the inter-alveolar septa thickness was assessed. Measurements were performed from the outer edge of the septum perpendicular to its axis.

For each animal, a semi-quantitative assessment of lung tissue damage was performed according to a modified scoring method by Carrol et al. [17]. The degree of involvement of the airways, lung parenchyma, and vascular bed was separately determined. Scoring criteria were defined for each section.

1. Damage to the airways was calculated by the total score of three pathological parameters, namely, (a) percentage of the affected airways (0, intact; 1, <10%; 2, 10%–25%; 3, 25%–50%; 4, >50%); (b) severity of airway damage (0, minimal peribronchial/peribronchiolar mononuclear infiltrates; 1, mild peribronchitis/bronchiolitis; 2, mild-to-moderate mononuclear or mixed cell peribronchiolitis; 3, severe mixed cell peribronchiolitis with large foci of the bronchiolar epithelium necrosis, but without atypical or multinucleated cells; 4, severe bronchiolitis and generalized epithelial necrosis and/or frequent atypical/syncytial cells); and (c) hyperplasia of the bronchiolar epithelium (0, intact; 1, sporadic hyperplasia of the bronchiolar epithelium <10% of the airway area; 2, mild-to-moderate bronchiolar epithelial hyperplasia; 10%–25% of the lumen of the airway area; 3, widespread hyperplasia of the bronchiolar epithelium and/or multinucleated syncytial cells occupying >25% of the airway area).
2. Damage to the lung parenchyma was calculated by the total score of three pathological parameters, namely, (a) percentage of the area of the affected alveoli (0, intact; 1, <10%; 2, 10%–25%; 3, 25%–50%; 4, >50%); (b) degree of alveolar injury (0, normal; 1, peribronchiolar primary mononuclear inflammatory infiltrates extending into adjacent alveolar septa/spaces; 2, mild-to-moderate mononuclear or mixed inflammation; 3, moderate mixed interstitial inflammation and/or alveolar damage characterized by necrosis/loss of type I pneumocytes with their replacement by hemorrhage, fibrin, edema, and necrotic remnants; 4, severe alveolar inflammation (mixed), damage to the alveolar septa, and loss of normal histoarchitecture with frequent syncytial cells); and (c) type II pneumocyte hyperplasia (0, none; 1, disseminated type II pneumocyte hyperplasia occupying <10% of the section; 2, mild-to-moderate type II pneumocyte hyperplasia occupying >10%–15% of atypical multinucleated cells; 3, generalized type II hyperplasia of pneumocytes occupying >25% of the section area).
3. Damage to the vascular bed was calculated by the total score of two pathological parameters, namely, (a) percentage of affected vessels on the section (0, none; 1, <10%; 2, 10%–25%; 3, 25%–50%; 4, >50%); and (b) vascular/perivascular lesions (0, intact; 1, mild multifocal perivascular edema/mononuclear perivascular inflammation; 2, moderate mononuclear or mixed cell perivascular inflammation, edema or fibrin with leukocytes sporadically transmigrating into the vessel wall/multifocal endothelitis; 3, severe mixed cell perivascular infiltration, edema/damage to the vessel wall, and/or severe frequent endothelitis).

Statistical processing of the results obtained was performed using analysis of variance with Tukey's correction for multiple comparisons. Differences were considered significant at $p < 0.05$.

Results

Infection of Syrian hamsters with SARS-CoV-2 lines B.1 (Wuhan) and B.1.617.2 (Delta) caused pronounced clinical symptoms; thus, the animals lost 12%–17% of their body weight, and their health worsened, which was expressed in general atony, tousled fur, lack of appetite, and reduced mobility (Fig. 1). Moreover, no significant differences were found in body weight changes over time between the two groups (Fig. 1*a*), whereas the clinical severity of the disease differed significantly. In general, the original strain B.1 group tolerated the infection worse than the B.1.617.2 group (Fig. 1*b*).

Determination of the viral load in animal tissues on day 5 after infection revealed significantly higher titers of strain B.1 than of B.1.617.2 both in the nasal passages and lungs, which is consistent with a more severe infection course in the B.1 group (Fig. 1*c*). No infectious virus was detected in other organs, which is consistent with the results of previously published studies [7, 9].

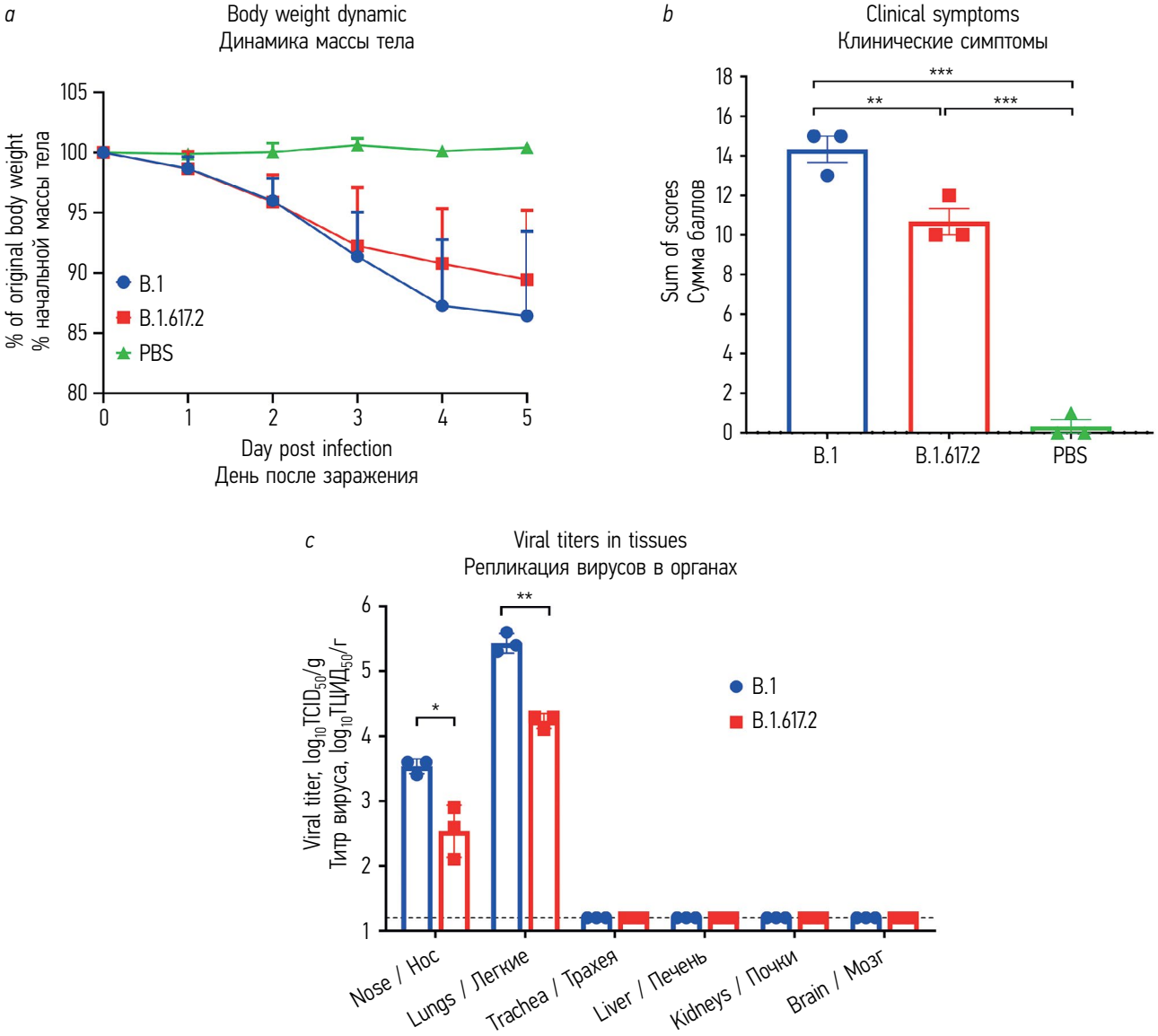

Fig. 1. Parameters of infection process on Syrian hamsters after SARS-CoV-2 inoculation (two lines B.1 and B.1.617.2) and placebo treatment with phosphate buffered saline: *a* — dynamics of body weight loss (0–5 days); *b* — integral clinical sum of scores (5 days); *c* — viral titer in nasal tissue, lings, trachea, liver, kidney and brain (log_{10} $TCID_{50}$/g tissue). ANOVA Tukey test: $*p < 0.05$; $**p < 0.01$; $***p < 0.001$

Рис. 1. Характеристика инфекционного процесса у сирийских хомяков, зараженных вирусами SARS-CoV-2 двух генетических линий B.1 и B.1.617.2, или получивших плацебо (PBS — фосфатно-солевой раствор): *a* — динамика изменения массы тела в течение 5 сут после заражения; *b* — интегральная оценка клинических проявлений болезни в течение 5 сут после заражения; *c* — детекция инфекционного вируса в различных тканях на 5-е сутки после заражения SARS-CoV-2. ANOVA с поправкой Тьюки на множественное сравнение: $*p < 0{,}05$; $**p < 0{,}01$; $***p < 0{,}001$

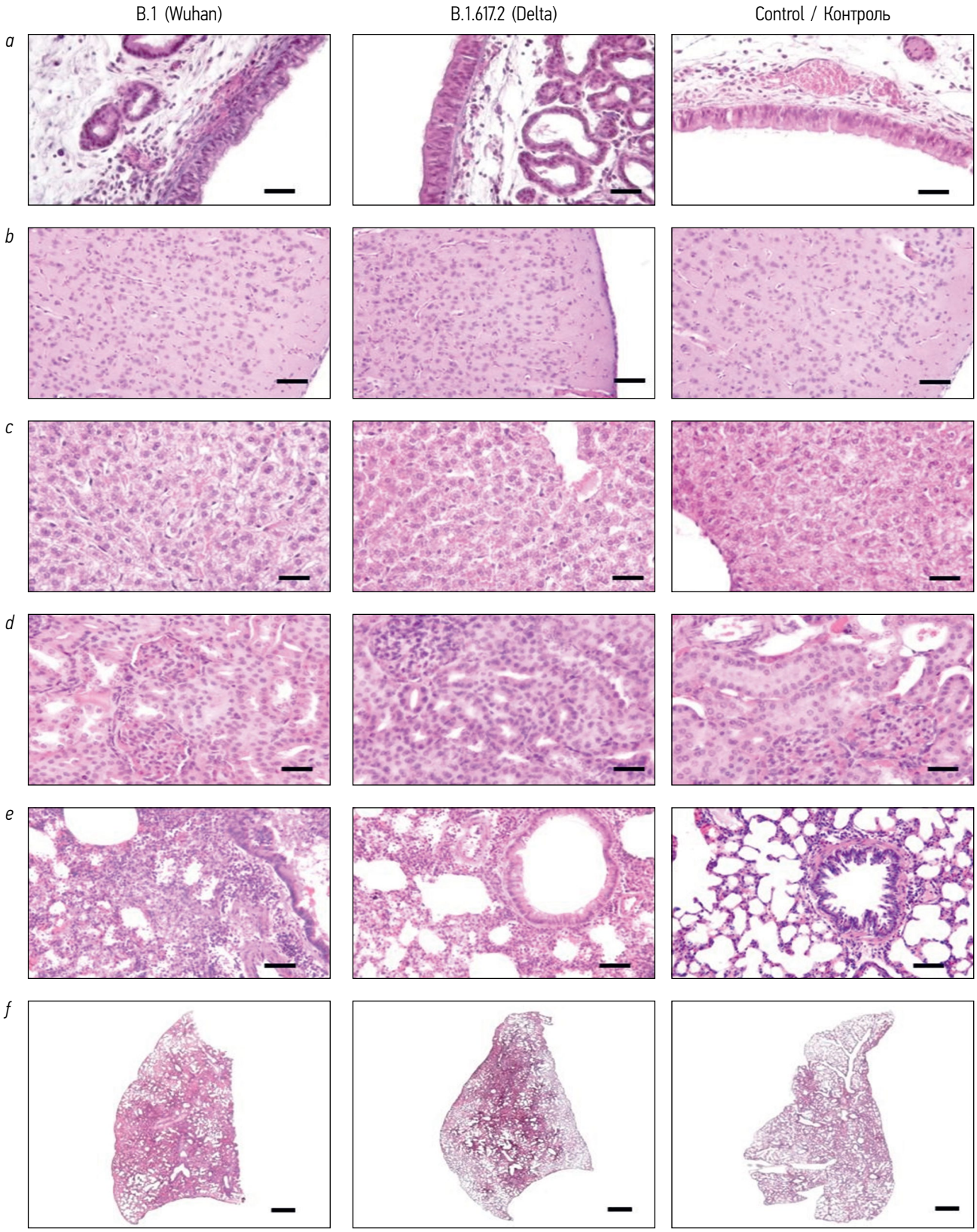

Fig. 2. Histopathologic changes of internal organs: *a* — trachea; *b* — brain cortex; *c* — liver; *d* — kidney. *e*, *f* — lungs after treatment with placebo (PBS, control) and two SARS-CoV-2 viruses — B.1 (Wuhan) and B.1.617.2 (Delta). H&E stain, 200 (*a*–*e*) and 50 (*f*) magnification with scale line 100 μm (*a*–*e*), 1 mm (*f*)

Рис. 2. Гистология внутренних органов хомяков, нормальная гистоархитектоника: *a* — трахея; *b* — кора головного мозга; *c* — печень; *d* — почка. *e*, *f* — срезы тканей легких контрольных животных (PBS), а также после заражения двумя вирусами SARS-CoV-2 — B.1 (Wuhan) и B.1.617.2 (Delta). Окраска гематоксилином и эозином, увеличение ×200, масштабная линейка 100 мкм (*a*–*e*), увеличение ×50, масштабная линейка 1 мм (*f*)

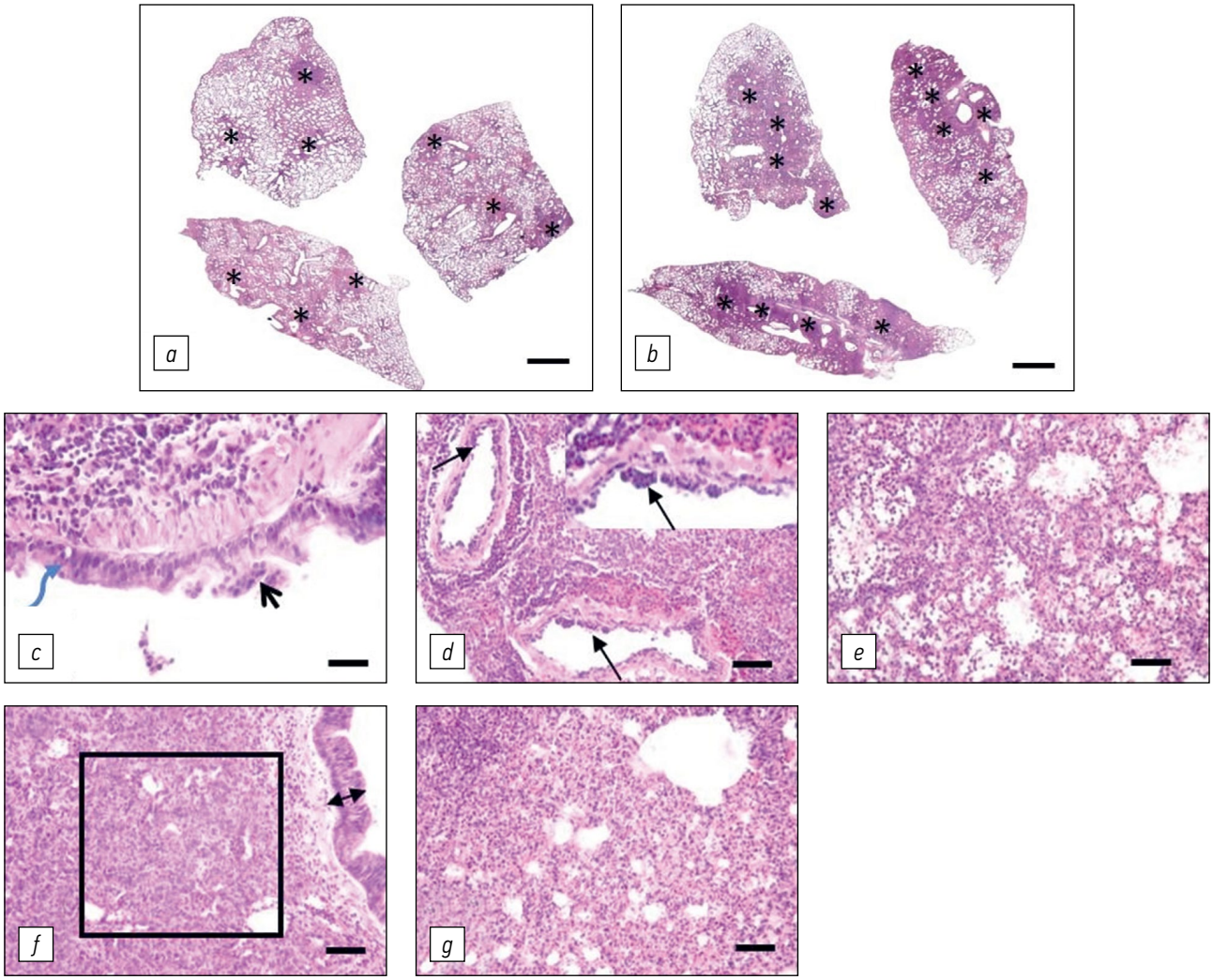

Fig. 3. Typical histopathologic features of the SARS-CoV-2 induced lung pathology: *a* — localized bronchogenic inflammatory foci; *b* — abundant inflammatory fields extending further in the lung tissue; asterisk — foci and/or diffuse mixed cell infiltrate; *c* — suppurative bronchiolitis — polymorphonuclear leukocytes and lymphocytes infiltrating partially ruptured bronchiolar wall; foci of necrotized (blue arrow) and syncytial multinucleated cell transformation (black arrow) bronchiolar epithelium; *d* — endothelialitis — endothelium lift off basal lamina by transmigrating inflammatory cells (arrows), severe vessel wall edema and abundant perivascular cuffing with mixed cell infiltrate; *e* — mononuclear infiltration and interalveolar septa thickening, prevailing intraalveolar edema with intraluminal hemorrhage, fibrin, cell debris and transmigrating macrophages; *f* — bronchiolar metaplasia of the alveolar epitelium, scattered type II pneumocyte hyperplasia amid the inflammatory alveolar lesion, also noted bronchiolar epithelium hyperplasia with cells pilling up (double arrow); *g* — diffuse alveolar damage — mixed inflammatory infiltrate: prevailing cells are lymphocytes, polymorphonuclear leukocytes and macrophages against the background of the intraalveolar edema and loss of structure. H&E stain, 50 magnification, scale line 2 mm (*a*–*b*), 200 magnification, scale line 100 μm (*c*–*g*)

Рис. 3. Характерные особенности патологических изменений тканей легких хомяков, инфицированных вирусом SARS-CoV-2: *a* — локализованные бронхогенные воспалительные фокусы; *b* — распространенные сливные воспалительные поля; звездочка — очаги смешанноклеточной инфильтрации легочной ткани; *c* — пример гнойно-некротического бронхиолита, стенка бронха инфильтрирована полиморфноядерными лейкоцитами и лимфоцитами, частично разрушена, фокусы некроза эпителия (голубая стрелка), гиперплазия, синцитиальная трансформация мерцательного эпителия (черная стрелка); *d* — сепарация эндотелия от базальной мембраны воспалительным инфильтратом (стрелки), отек медии и массивный перивазальный смешанно-клеточный инфильтрат; *e* — утолщение межальвеолярных перегородок за счет мононуклеарной инфильтрации и отека, фибрин, клеточный детрит и макрофагальная инфильтрация в просвете альвеол, обширное интраальвеолярное кровоизлияние; *f* — указан фокус бронхиолярной метаплазии альвеолярного эпителия, также встречается рассеянная гиперплазия альвеолоцитов II типа на фоне смешанноклеточной инфильтрации межальвеолярных перегородок, гиперплазия бронхиолярного эпителия (двойная стрелка); *g* — диффузное альвеолярное повреждение — смешанно-клеточный воспалительный инфильтрат, состоящий преимущественно из лимфоцитов, полиморфнонуклеарных лейкоцитов, макрофагов на фоне клеточного детрита и разрушенных альвеол. Окраска гематоксилином и эозином, увеличение ×50, масштабная линейка 2 мм (*a*–*b*), увеличение ×200, масштабная линейка 100 мкм (*c*–*g*)

In all groups, the tracheal histoarchitecture corresponded to the species norm. The epithelial cover was represented by a single layer of multi-row ciliated epithelium. Cilia on the apical surface of epitheliocytes were preserved throughout the layer. The count of the goblet cells did not increase. In the lamina propria, single lymphocytes were determined, and the vessels were moderately plethorical (Fig. 2*a*). Histological evaluation of the brain, liver, and kidneys also did not reveal inflammatory or dystrophic changes. The histoarchitecture of the organs of all the studied individuals corresponded to the species norm (Fig. 2*b*–*d*). Analysis of histological sections of the lung tissues of hamsters revealed pathological changes in animals infected with B.1 and B.1.617.2. The pathology of the lung tissue was of the same nature in both groups. The B.1 group (Wuhan) had a more pronounced degree of lesion than the B.1.617.2 group (Fig. 2*e, f*). As expected, the histoarchitecture of the lungs of the control group animals corresponded to the norm (Fig. 2*e, f*).

The most significant characteristic changes in the histological pattern of lung tissues in SARS-CoV-2-infected Syrian hamsters of both study groups are presented in Fig. 3. A panoramic image at a low magnification ×50 demonstrated large peribronchial and perivasal inflammatory foci, areas of the lung tissue consolidation, and large foci of intra-alveolar hemorrhages in all samples of the experimental groups. Extensive subpleural areas of the lungs were emphysematously transformed. Sites of inflammatory infiltration were focal and localized (Fig. 3*a*). Confluent areas of pneumonia, occupying a significant section area, were also defined (Fig. 3*b*). Despite the more pronounced nature of lung damage in the B.1 group, the morphometric analysis revealed no significant differences between the two strains of SARS-CoV-2 in terms of the area of inflammatory infiltrates, presumably due to the small number of animals in each group (Fig. 4*a*).

With an increase of ×200, sections of the bronchi and bronchiole lumen of the infected animals reveal a significant amount of exudate and cellular detritus with lymphohistiocytic admixture. The bronchiolar epithelium is hyperplastic, swollen, with foci of necrosis and formation of giant multicellular syncytia (Fig. 3*c*). Mixed cell lymphohistiocytic infiltrates are located subepithelially in the bronchus wall, partially lysing it, and proliferate into the surrounding parenchyma. Moreover, a semi-quantitative integral assessment of the severity of airway lesion did not reveal differences in the degree of involvement of the bronchi and bronchioles in the pathological process in the B.1 and B.1.617.2 groups (Fig. 4*b*).

The vessels on lung sections of infected hamsters were unevenly plethoric. The vascular endothelium was edematous, partially separated from the basement membrane by accumulations of lymphocytes and polymorphonuclear leukocytes (Fig. 3*d*). The media and adventitia were edematous and significantly infiltrated. Extensive mixed cell infiltrates proliferated perivasally. Moreover, a semi-quantitative assessment of vascular damage did not reveal significant differences between the two groups (Fig. 4*c*).

The inter-alveolar septa in most fields of vision were edematous, infiltrated with lymphocytes and polymorphonuclear leukocytes (Fig. 3*e*). If a semi-quantitative assessment of pulmonary/alveolar pathology did not reveal significant differences between SARS-CoV-2 strains B.1 and B.1.617.2 (Fig. 4*d*), then a morphometric analysis of the inter-alveolar septa thickness showed a significant increase in this indicator in the B.1 group than in the B.1.617.2 group, whereas the findings in both groups differed significantly from the control samples (Fig. 4*e*).

In addition to the lesions described above, foci of bronchiolar metaplasia of the alveolar epithelium and areas of hyperplasia of type II alveolocytes were identified (Fig. 3*f*). In areas with most severe damage, the inter-alveolar septa were destroyed, the respiratory space was filled with fibrin, cellular detritus, and a massive polymorphocellular infiltrate (Fig. 3*g*). Morphometric assessment of the airspace by MLI measurement demonstrated heterogeneous lung tissue damage in the experimental subgroups (Fig. 4*f*). A large dispersion of the MLI index was associated with a significant spread of emphysematous expanded fields accompanied by a collapse of the lung tissue on the periphery of the pneumonic foci. Accordingly, the MLI cannot be considered informative in the pathomorphological study of SARS-CoV-2-induced lung pathology in Syrian hamsters because it does not allow identifying differences between the two virus strains that differ significantly in the clinical severity in this animal model.

Discussion

In this study, we revealed that coronaviruses replicated actively in the nasal passages and lungs of Syrian hamsters, demonstrating a pronounced clinical presentation [18–22]. COVID-19 causes specific lesions in lung tissues; therefore, the published works most often present studies of the involvement of lung tissues (percentage of lesions) or an integral assessment of lesions by a scoring system.

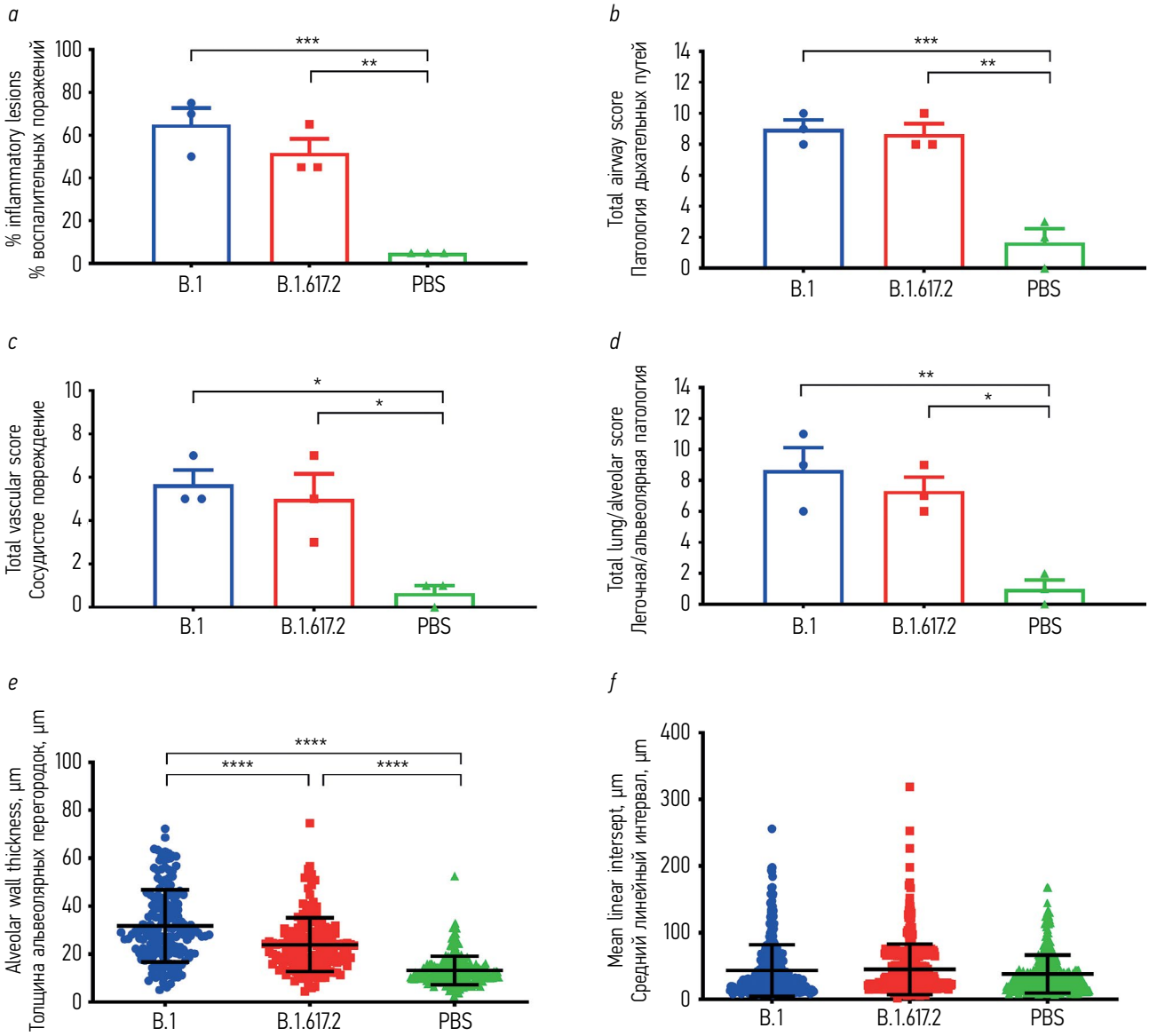

Fig. 4. Morphometric lung data, obtained at 5th day after SARS-CoV-2 infection: *a* — percentage of the lung tissue affected by the inflammatory lesions; *b* — airway semiquantitative assessment; *c* — vessel bed semiquantitative assessment; *d* — alveolar lesions semiquantitative assessment; *e* — alveolar wall thickness; *f* — MLI. PBS — phosphate buffered saline. ANOVA Tukey test: * $p < 0.05$; ** $p < 0.01$; *** $p < 0.001$; **** $p < 0.0001$

Рис. 4. Морфометрические показатели патологических изменений в тканях легких сирийских хомяков на 5-й день после заражения SARS-CoV-2: *a* — вовлеченность легочной ткани в воспалительный процесс, %; *b* — полуколичественный анализ патологии воздухоносных путей; *c* — полуколичественный анализ сосудистых поражений; *d* — полуколичественный анализ легочной/альвеолярной патологии; *e* — толщина межальвеолярных перегородок; *f* — показатель MLI. PBS — фосфатно-солевой раствор. ANOVA с поправкой Тьюки на множественное сравнение: * $p < 0,05$; ** $p < 0,01$; *** $p < 0,001$; **** $p < 0,0001$

In a detailed study of pathomorphological changes in the lung tissues of Syrian hamsters with COVID-19, we inoculated two SARS-CoV-2 strains that differ in the clinical severity of the disease. Since the two viruses have different clinical presentation and specific pathological changes were detected only in lung tissues, revealing such morphometric parameters that would indicate the degree of the pathogenicity of the virus was important. Thus, in the future, the protective effect of prophylactic and therapeutic drugs on this animal model should be evaluated. In our study, no significant differences were found in the MLI between the two studied strains and in the integral semi-quantitative assessments of lung pathology at the level of the airways and alveolar and vascular lesions. An extended morphometric analysis of various pathological changes in lung tissues showed that the measurement of the thickness of the inter-alveolar septa turned out to be the most sensitive criterion for the degree of

lung damage in Syrian hamsters with COVID-19. Thickening of the inter-alveolar septa during the exudative phase of diffuse alveolar injury is predominantly caused by edema, leukocyte migration, and pneumocyte hyperplasia. This process is stereotypical and is noted in a wide range of pulmonary pathologies, especially those of infectious origin. However, this parameter, even with a small number of animals in the group, enables us to identify significant differences between experimental animals exhibiting different clinical disease severities.

Conclusion

This study demonstrates that the SARS-CoV-2 delta virus (B.1.617.2) is less pathogenic for Syrian hamsters than B.1, the original strain circulating during the first wave of the COVID-19 pandemic. A thorough histopathological characterization of lung tissue sections of infected animals would allow us to identify the most sensitive morphometric indicator that reflects the severity of SARS-CoV 2-induced pathology, such as inter-alveolar septa thickness. This indicator enables us to determine even slight differences in the severity of virus-induced pathology and can be used in preclinical studies of prophylactic and therapeutic drugs for the treatment of COVID-19.

Additional information

Funding sources. The study was funded by the Russian Science Foundation grant No. 21-75-30003.

Compliance with ethical standards. The study was approved by the local Ethical Committee of the Institute of Experimental Medicine (No. 1/22 by 18.02.2022).

Competing interests. The authors declare the absence of obvious and potential conflicts of interest related to the publication of this article.

Authors' contribution. All authors made a significant contribution to the development of the concept and preparation of the article, read and approved the final version before publication. The largest contribution is distributed as follows: *I.N. Isakova-Sivak* — concept, research plan; *K.S. Yakovlev, D.A. Mezhenskaya, K.V. Sivak* — conducting experiments, their interpretation; *L.G. Rudenko* — project administration and data analysis.

Дополнительная информация

Источник финансирования. Исследование выполнено при поддержке Российского научного фонда (грант № 21-75-30003).

Соблюдение этических норм. Исследование одобрено на заседании локального этического комитета ФГБНУ «Института экспериментальной медицины» (№ 1/22 от 18.02.2022).

Конфликт интересов. Авторы декларирует отсутствие явных и потенциальных конфликтов интересов, связанных с подготовкой и публикацией настоящей статьи.

Вклад авторов. Все авторы внесли существенный вклад в разработку концепции, проведение исследования и подготовку статьи, прочли и одобрили финальную версию перед публикацией. Наибольший вклад распределен следующим образом: *И.Н. Исакова-Сивак* — идея, план исследований; *К.С. Яковлев, Д.А. Меженская, К.В. Сивак* — проведение экспериментов, анализ данных; *Л.Г. Руденко* — общее руководство, обсуждение результатов.

References

1. Zhu N, Zhang D, Wang W, et al. A novel coronavirus from patients with pneumonia in China, 2019. *N Engl J Med.* 2020;382(8):727–733. DOI: 10.1056/NEJMoa2001017
2. Anonymous. Worldometer of COVID-19 coronavirus pandemic [Internet]. Available from: https://www.worldometers.info/coronavirus/. Accessed: June 13, 2022.
3. Chu H, Chan JF, Yuen KY. Animal models in SARS-CoV-2 research. *Nat Methods.* 2022;19(4):392–394. DOI: 10.1038/s41592-022-01447-w
4. Munoz-Fontela C, Dowling WE, Funnell SGP, et al. Animal models for COVID-19. *Nature.* 2020;586(7830):509–515. DOI: 10.1038/s41586-020-2787-6
5. Bednash JS, Kagan VE, Englert JA, et al. Syrian hamsters as a model of lung injury with SARS-CoV-2 infection: Pathologic, physiologic, and detailed molecular profiling. *Transl Res.* 2022;240:1–16. DOI: 10.1016/j.trsl.2021.10.007
6. Sia SF, Yan LM, Chin AWH, et al. Pathogenesis and transmission of SARS-CoV-2 in golden hamsters. *Nature.* 2020;583(7818):834–838. DOI: 10.1038/s41586-020-2342-5
7. Imai M, Iwatsuki-Horimoto K, Hatta M, et al. Syrian hamsters as a small animal model for SARS-CoV-2 infection and countermeasure development. *Proc Natl Acad Sci USA.* 2020;117(28):16587–16595. DOI: 10.1073/pnas.2009799117
8. Mohandas S, Yadav PD, Shete A, et al. SARS-CoV-2 delta variant pathogenesis and host response in Syrian hamsters. *Viruses.* 2021;13(9):1773. DOI: 10.3390/v13091773
9. Francis ME, Goncin U, Kroeker A, et al. SARS-CoV-2 infection in the Syrian hamster model causes inflammation as well as type I interferon dysregulation in both respiratory and non-respiratory tissues including the heart and kidney. *PLoS Pathog.* 2021;17(7):e1009705. DOI: 10.1371/journal.ppat.1009705
10. Moghaddar M, Radman R, Macreadie I. Severity, pathogenicity and transmissibility of delta and lambda variants of

SARS-CoV-2, toxicity of spike protein and possibilities for future prevention of COVID-19. *Microorganisms.* 2021;9(10):2167. DOI: 10.3390/microorganisms9102167
11. Yuan S, Ye ZW, Liang R, et al. Pathogenicity, transmissibility, and fitness of SARS-CoV-2 Omicron in Syrian hamsters. *Science*. 2022;377(6604):428–433. DOI: 10.1126/science.abn8939
12. Matyushenko V, Isakova-Sivak I, Kudryavtsev I, et al. Detection of IFNgamma-secreting CD4(+) and CD8(+) memory t cells in COVID-19 convalescents after stimulation of peripheral blood mononuclear cells with live SARS-CoV-2. *Viruses*. 2021;13(8):1490. DOI: 10.3390/v13081490
13. Sokolov A, Isakova-Sivak I, Grudinina N, et al. Ferristatin II efficiently inhibits SARS-CoV-2 replication in vero cells. *Viruses*. 2022;14(2):317. DOI: 10.3390/v14020317
14. Reed LJ, Muench H. A Simple method of estimating fifty per cent endpoints. *Am J Epidemiol*. 1938;27(3):493–497. DOI: 10.1093/oxfordjournals.aje.a118408
15. Directive 2010/63/EU of the European Parliament 263 and of the Council 264 of 22 September 2010 on the protection of animals used for scientific purposes. *Official Journal of the European Union.* 2010;53:33–79.
16. Hsia CC, Hyde DM, Ochs M, et al. An official research policy statement of the American Thoracic Society/European Respiratory Society: standards for quantitative assessment of lung structure. *Am J Respir Crit Care Med*. 2010;181(4):394–418. DOI: 10.1164/rccm.200809-1522ST
17. Carroll T, Fox D, van Doremalen N, et al. The B.1.427/1.429 (epsilon) SARS-CoV-2 variants are more virulent than ancestral B.1 (614G) in Syrian hamsters. *PLoS Pathog.* 2022;18(2):e1009914. DOI: 10.1371/journal.ppat.1009914
18. Fischer RJ, van Doremalen N, Adney DR, et al. ChAdOx1 nCoV-19 (AZD1222) protects Syrian hamsters against SARS-CoV-2 B.1.351 and B.1.1.7. *bioRxiv.* 2021. DOI: 10.1101/2021.03.11.435000
19. Van der Lubbe JEM, Rosendahl Huber SK, Vijayan A, et al. Ad26.COV2.S protects Syrian hamsters against G614 spike variant SARS-CoV-2 and does not enhance respiratory disease. *NPJ Vaccines*. 2021;6(1):39. DOI: 10.1038/s41541-021-00301-y
20. Tamming LA, Duque D, Tran A, et al. DNA based vaccine expressing SARS-CoV-2 Spike-CD40L fusion protein confers protection against challenge in a Syrian hamster model. *Front Immunol.* 2021;12:785349. DOI: 10.3389/fimmu.2021.785349
21. Johnson S, Martinez CI, Tedjakusuma SN, et al. Oral vaccination protects against severe acute respiratory syndrome coronavirus 2 in a Syrian hamster challenge model. *J Infect Dis.* 2022;225(1):34–41. DOI: 10.1093/infdis/jiab561
22. Kulkarni R, Chen WC, Lee Y, et al. Vaccinia virus-based vaccines confer protective immunity against SARS-CoV-2 virus in Syrian hamsters. *PLoS One.* 2021;16(9):e0257191. DOI: 10.1371/journal.pone.0257191

Список литературы

1. Zhu N., Zhang D., Wang W. et al. A novel coronavirus from patients with pneumonia in China, 2019 // N. Engl. J. Med. 2020. Vol. 382, No. 8. P. 727–733. DOI: 10.1056/NEJMoa2001017
2. Anonymous. Worldometer of COVID-19 coronavirus pandemic [Электронный ресурс]. Режим доступа: https://www.worldometers.info/coronavirus/. Дата обращения: 13.06.2022.
3. Chu H., Chan J.F., Yuen K.Y. Animal models in SARS-CoV-2 research // Nat Methods. 2022. Vol. 19, No. 4. P. 392–394. DOI: 10.1038/s41592-022-01447-w
4. Munoz-Fontela C., Dowling W.E., Funnell S.G.P. et al. Animal models for COVID-19 // Nature. 2020. Vol. 586, No. 7830. P. 509–515. DOI: 10.1038/s41586-020-2787-6
5. Bednash J.S., Kagan V.E., Englert J.A. et al. Syrian hamsters as a model of lung injury with SARS-CoV-2 infection: Pathologic, physiologic, and detailed molecular profiling // Transl. Res. 2022. Vol. 240. P. 1–16. DOI: 10.1016/j.trsl.2021.10.007
6. Sia S.F., Yan L.M., Chin A.W.H. et al. Pathogenesis and transmission of SARS-CoV-2 in golden hamsters // Nature. 2020. Vol. 583, No. 7818. P. 834–838. DOI: 10.1038/s41586-020-2342-5
7. Imai M., Iwatsuki-Horimoto K., Hatta M. et al. Syrian hamsters as a small animal model for SARS-CoV-2 infection and countermeasure development // Proc. Natl. Acad. Sci. USA. 2020. Vol. 117, No. 28. P. 16587–16595. DOI: 10.1073/pnas.2009799117
8. Mohandas S., Yadav P.D., Shete A. et al. SARS-CoV-2 delta variant pathogenesis and host response in Syrian hamsters // Viruses. 2021. Vol. 13, No. 9. P. 1773. DOI: 10.3390/v13091773
9. Francis M.E., Goncin U., Kroeker A. et al. SARS-CoV-2 infection in the Syrian hamster model causes inflammation as well as type I interferon dysregulation in both respiratory and non-respiratory tissues including the heart and kidney // PLoS Pathog. 2021. Vol. 17, No. 7. P. e1009705. DOI: 10.1371/journal.ppat.1009705
10. Moghaddar M., Radman R., Macreadie I. Severity, pathogenicity and transmissibility of delta and lambda variants of SARS-CoV-2, toxicity of spike protein and possibilities for future prevention of COVID-19 // Microorganisms. 2021. Vol. 9, No. 10. P. 2167. DOI: 10.3390/microorganisms9102167
11. Yuan S., Ye Z.W., Liang R. et al. Pathogenicity, transmissibility, and fitness of SARS-CoV-2 Omicron in Syrian hamsters // Science. 2022. Vol. 377, No. 6604. P. 428–433. DOI: 10.1126/science.abn8939
12. Matyushenko V., Isakova-Sivak I., Kudryavtsev I. et al. Detection of IFNgamma-secreting CD4(+) and CD8(+) memory t cells in COVID-19 convalescents after stimulation of peripheral blood mononuclear cells with live SARS-CoV-2 // Viruses. 2021. Vol. 13, No. 8. P. 1490. DOI: 10.3390/v13081490
13. Sokolov A., Isakova-Sivak I., Grudinina N. et al. Ferristatin II efficiently inhibits SARS-CoV-2 replication in vero cells // Viruses. 2022. Vol. 14, No. 2. P. 317. DOI: 10.3390/v14020317
14. Reed L.J., Muench H. A Simple method of estimating fifty per cent endpoints // Am. J. Epidemiol. 1938. Vol. 27, No. 3. P. 493–497. DOI: 10.1093/oxfordjournals.aje.a118408
15. Directive 2010/63/EU of the European Parliament 263 and of the Council 264 of 22 September 2010 on the protection of animals used for scientific purposes // Official Journal of the European Union. 2010. Vol. 53. P. 33–79.
16. Hsia C.C., Hyde D.M., Ochs M. et al. An official research policy statement of the American Thoracic Society/European Respiratory Society: standards for quantitative assessment of lung

structure // Am. J. Respir. Crit. Care Med. 2010. Vol. 181, No. 4. P. 394–418. DOI: 10.1164/rccm.200809-1522ST
17. Carroll T., Fox D., van Doremalen N. et al. The B.1.427/1.429 (epsilon) SARS-CoV-2 variants are more virulent than ancestral B.1 (614G) in Syrian hamsters // PLoS Pathog. 2022. Vol. 18, No. 2. P. e1009914. DOI: 10.1371/journal.ppat.1009914
18. Fischer R.J., van Doremalen N., Adney D.R. et al. ChAdOx1 nCoV-19 (AZD1222) protects Syrian hamsters against SARS-CoV-2 B.1.351 and B.1.1.7 // bioRxiv. 2021. DOI: 10.1101/2021.03.11.435000
19. Van der Lubbe J.E.M., Rosendahl Huber S.K., Vijayan A. et al. Ad26.COV2.S protects Syrian hamsters against G614 spike variant SARS-CoV-2 and does not enhance respiratory disease // NPJ Vaccines. 2021. Vol. 6, No. 1. P. 39. DOI: 10.1038/s41541-021-00301-y
20. Tamming L.A., Duque D., Tran A. et al. DNA based vaccine expressing SARS-CoV-2 Spike-CD40L fusion protein confers protection against challenge in a Syrian hamster model // Front. Immunol. 2021. Vol. 12. P. 785349. DOI: 10.3389/fimmu.2021.785349
21. Johnson S., Martinez C.I., Tedjakusuma S.N. et al. Oral vaccination protects against severe acute respiratory syndrome coronavirus 2 in a Syrian hamster challenge model // J. Infect. Dis. 2022. Vol. 225, No. 1. P. 34–41. DOI: 10.1093/infdis/jiab561
22. Kulkarni R., Chen W.C., Lee Y. et al. Vaccinia virus-based vaccines confer protective immunity against SARS-CoV-2 virus in Syrian hamsters // PLoS One. 2021. Vol. 16, No. 9. P. e0257191. DOI: 10.1371/journal.pone.0257191

Information about the authors / Информация об авторах

Smorodintsev Research Institute of Influenza, Saint Petersburg, Russia
ФГБУ «Научно-исследовательский институт гриппа им. А.А. Смородинцева» Минздрава России, Санкт-Петербург, Россия

Kirill S. Yakovlev — Research Assistant at the Department of Preclinical Trials.
ORCID: https://orcid.org/0000-0001-7000-3467;
e-mail: kirikus-fly@yandex.ru

Кирилл Сергеевич Яковлев — лаборант-исследователь отдела доклинических исследований.
ORCID: https://orcid.org/0000-0001-7000-3467;
e-mail: kirikus-fly@yandex.ru

Konstantin V. Sivak — Cand. Sci. (Biol.), Head of the Department of Preclinical Trials.
ORCID: https://orcid.org/0000-0003-4064-5033;
Scopus Author ID: 35269910300;
e-mail: kvsivak@gmail.com

Константин Владимирович Сивак — канд. биол. наук, заведующий отделом доклинических исследований.
ORCID: https://orcid.org/0000-0003-4064-5033;
Scopus Author ID: 35269910300;
e-mail: kvsivak@gmail.com

Institute of Experimental Medicine, Saint Petersburg, Russia
ФГБНУ «Институт экспериментальной медицины», Санкт-Петербург, Россия

Daria A. Mezhenskaya — Research Associate of Laboratory of Immunology and Prevention of Viral Infections, A.A. Smorodintsev Department of Virology.
ORCID: https://orcid.org/0000-0001-6922-7682;
Scopus Author ID: 57188763106;
eLibrary SPIN: 5799-8802; e-mail: dasmez@iemspb.ru

Дарья Андреевна Меженская — научный сотрудник лаборатории иммунологии и профилактики вирусных инфекций отдела вирусологии им. А.А. Смородинцева.
ORCID: https://orcid.org/0000-0001-6922-7682;
Scopus Author ID: 57188763106;
eLibrary SPIN: 5799-8802; e-mail: dasmez@iemspb.ru

Larisa G. Rudenko — MD, Dr. Sci. (Med.), Professor, Head of Department of Virology, A.A. Smorodintsev Department of Virology.
ORCID: https://orcid.org/0000-0002-0107-9959;
Scopus Author ID: 7005033248;
eLibrary SPIN: 4181-1372; e-mail: vaccine@mail.ru

Лариса Георгиевна Руденко — д-р мед. наук, профессор, заведующая отделом вирусологии им. А.А. Смородинцева.
ORCID: https://orcid.org/0000-0002-0107-9959;
Scopus Author ID: 7005033248;
eLibrary SPIN: 4181-1372; e-mail: vaccine@mail.ru

Information about the authors / Информация об авторах

Irina N. Isakova-Sivak — Dr. Sci. (Biol.), Head of Laboratory of Immunology and Prevention of Viral Infections, A.A. Smorodintsev Department of Virology.
ORCID: https://orcid.org/0000-0002-2801-1508;
Scopus Author ID: 23973026600;
eLibrary SPIN: 3469-3600;
e-mail: isakova.sivak@iemspb.ru

Ирина Николаевна Исакова-Сивак — д-р биол. наук, заведующая лабораторией иммунологии и профилактики вирусных инфекций отдела вирусологии им. А.А. Смородинцева.
ORCID: https://orcid.org/0000-0002-2801-1508;
Scopus Author ID: 23973026600;
eLibrary SPIN: 3469-3600;
e-mail: isakova.sivak@iemspb.ru

✉ **Corresponding author / Контактное лицо**

Daria A. Mezhenskaya / Дарья Андреевна Меженская
Address: 12 Academician Pavlov St., Saint Petersburg, 197022, Russia
Адрес: Россия, 197022, Санкт-Петербург, ул. Академика Павлова, д. 12
E-mail: dasmez@iemspb.ru